ACCOUNTS
of chemical research

Photoinduced Dynamics in Semiconductor Quantum Dots: Insights from Time-Domain *ab Initio* Studies

OLEG V. PREZHDO*

Department of Chemistry, University of Washington, Seattle, Washington 98195-1700

RECEIVED ON MAY 27, 2009

CONSPECTUS

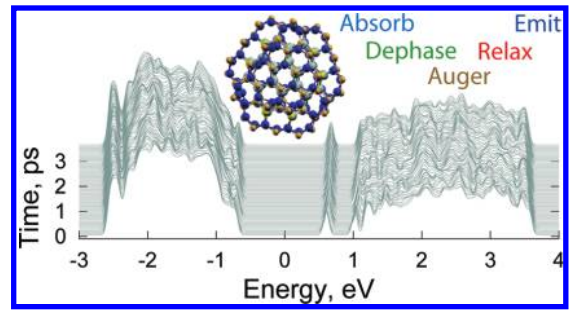

Nanoscale clusters of bulk materials, also known as quantum dots (QDs), exhibit both molecular and bulk properties. Unlike either bulk or molecular materials, QD properties can be modified continuously by changing QD shape and size. However, the chemical and physical properties of molecular and bulk materials often contradict each other, which can lead to differing viewpoints about the behavior of QDs. For example, the molecular view suggests strong electron−hole and charge−phonon interactions, as well as slow energy relaxation due to mismatch between electronic energy gaps and phonon frequencies. In contrast, the bulk view advocates that the kinetic energy of quantum confinement is greater than electron−hole interactions, that charge−phonon coupling is weak, and that the relaxation through quasi-continuous bands is rapid. By synthesizing the bulk and molecular viewpoints, this Account clarifies the controversies and provides a unified atomistic picture of the nature and dynamics of photoexcited states in semiconductor QDs. Based on the state-of-the-art *ab initio* approaches in both the energy and time domains, the Account presents a comprehensive discussion of the dynamical processes in QDs, ranging from the initial photon absorption to the final emission.

The atomistic description of QDs complements phenomenological models, provides important details, and creates new scientific paradigms. The *ab initio* approaches are particularly useful for studying geometric and electronic structure of QDs because they treat bulk, surface, ligands, and defects on equal footing and incorporate electronic correlation effects. Nonadiabatic molecular dynamics simulations most closely mimic the complex coupled evolutions of charges, phonons, and spins as they occur in nature. The simulations show that the underlying atomic structure, thermal fluctuations, and surface effects lift electronic state degeneracies predicted by phenomenological models and that excitonic electron−hole interactions are strong in small QDs.

Stoichiometric surfaces self-heal. However, only molecular ligands and core/shell designs can eliminate traps associated with dangling chemical bonds, missing atoms, and other defects. Ligands create charge traps and provide high-frequency phonons. The phonon-induced dephasing of electronic excitations is ultrafast, ranging from tens to hundreds of femtoseconds.

The dependence of the relaxation on the excitation energy and the density of states clarify the controversies regarding the phonon bottleneck in the photoexcited electron relaxation, and the participation of low-frequency phonons explains the temperature dependence of the relaxation rate. We rationalize the ultrafast generation of multiple excitons without the phononbottleneck by strong Coulomb interactions between the charge carriers. The QD charging and defects explain the large variation in the experimental data on multiple exciton generation.

The issues raised here with the electronic states and semiconductor QDs are similar to those found with the spin states and metallic QDs. Assemblies of QDs with other materials, such as organic chromophores and inorganic semiconductors, will present new sets of questions. Time-domain *ab initio* approaches will allow scientists to address these challenges directly in the near future.

Published on the Web 11/04/2009 www.pubs.acs.org/acr
10.1021/ar900157s CCC: $71.50

Introduction

Nanoscale clusters of bulk materials, also known as quantum dots (QDs), exhibit the remarkable property of quantum confinement. This phenomenon allows one to continuously tune various properties by changing cluster size and shape. QDs are in sharp contrast with molecular systems, whose properties vary discontinuously and require modifications in composition and structure. The QD size below which quantum confinement becomes important is given by the extent of electronic excitation in bulk. This so-called Bohr exciton radius is in the range of a few nanometers to tens of nanometers for typical semiconductors. Collective excitations in metallic nanoparticles, for example, plasmons, can be tuned at a much larger particle size. On the subnanometer scale, clusters become molecular-like. Their structure can deviate from bulk, and their properties change discontinuously with cluster size.

Dynamics of electronic excitations in semiconducting[1] and metallic[2] QDs is quite complex. It underlies many applications, including light-emitting diodes,[3] field-effect transistors,[4] lasers,[5] quantum antennas,[6] biological probes,[7] quantum information devices,[8] spintronic systems,[9] and thermopower machines.[10] High absorption cross sections, decreased electron−phonon relaxation rates,[11,12] and generation of multiple electron−hole pairs[13−15] make QDs excellent photovoltaic materials.[11,16] Electron−hole and charge−phonon interactions carry both fundamental and practical importance. For example, QD photovoltaic and lasing efficiencies depend on the rates of electron−hole energy exchange and charge−phonon relaxation. Quantum information processing is limited by phonon-induced dephasing of spin and electron states. Inelastic scattering is responsible for transport blockade and energy loss during charge tunneling through QDs.

QDs are studied by several scientific communities and can be viewed alternatively as reduced-dimensional bulk or scaled-up molecular systems. Similar to molecules, QDs show discrete optical transitions. Similar to bulk, QDs comprise multiple unit cells and form electronic and vibrational bands. The charge−phonon and electron−hole interactions are weaker in QDs than in molecules but are stronger than those in bulk. Often, the molecular and bulk viewpoints use different terminology to describe the same phenomenon and even generate contradictions. For instance, electron-correlation effects known in chemistry translate into excitonic electron−hole interactions in physics. The molecular view suggests that excitonic and charge−phonon interactions are strong and that relaxation is slow due to mismatch between electron and phonon energies. In contrast, the bulk view indicates that kinetic energy of quantum confinement is significantly greater than excitonic interactions and that charge−phonon relaxation through quasi-continuous bands is rapid. Such qualitative differences create debates that must be settled in order to advance both fundamental understanding and applications of QDs.

This Account presents an *ab initio* description of the nature and dynamics of photoexcited states in semiconductor QDs, in both energy and time domains. By synthesizing the bulk and molecular viewpoints, the analysis clarifies the controversies and provides a unified atomistic picture of the excited state processes, Figure 1.

Theoretical Approaches

The results discussed below are obtained with *ab initio* methods. Other approaches include effective-mass theory[11,14] (EMT) and pseudopotential technique.[17−19] Historically first, EMT develops a particle-in-a-box model with electron and hole masses given by their bulk values. An intuitive description, EMT explains general trends seen in experiments. The atomistic pseudopotential technique can be applied to large systems, but requires careful parametrization for each material. *Ab initio* approaches are particularly valuable for studying dopants, defects, ligands, core/shell systems, and QD synthesis. They use minimal parametrization and are applicable to most materials across the periodic table. The Hartree−Fock (HF) method and density functional theory (DFT) date back many decades. Time-domain (TD) DFT and nonadiabatic molecular dynamics (NAMD) are more active areas of research. Currently, *ab initio* TDDFT/NAMD is the only technique that models QD dynamics in the time domain and at atomistic level, directly mimicking time-resolved experiments.

A Single-Particle Theory, Hartree−Fock Describes Interaction of an Electron with the Mean Field Created by Other Electrons. HF approximates Schrödinger's equation for a multidimensional wave function with coupled three-variable equations for single-electron orbitals. For example, a wave function describing valence electrons in a 500 atom Si QD contains 6000 variables. Single-particle HF equations depend on 3 variables and provide a great simplification. Electron−electron repulsion is included as mean-field: each electron sees an average cloud created by remaining electrons, Figure 2. HF achieves self-consistency, since electron orbitals are determined by mean field and mean field depends on the orbitals. HF incorporates Pauli exclusion through the exchange interaction, which does not allow two identical electrons to occupy the same location.

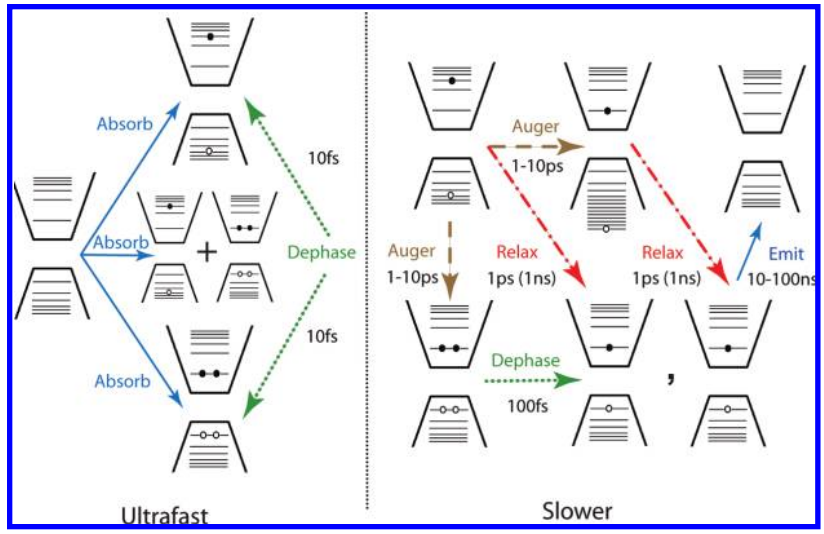

FIGURE 1. Photoinduced electron−phonon dynamics in semiconductor QDs. An absorbed photon excites one or multiple electron−hole pairs or superpositions thereof. Superpositions rapidly dephase by coupling to phonons. Multiple electron−hole pairs dephase into independent single electron−hole pairs on a slower time scale. Auger processes exchange energy between electrons and holes and can create additional electron−hole pairs. Besides dephasing, electron−phonon coupling causes nonradiative relaxation, converting excitation energy to heat. Ultimately, all decay channels lead to uncorrelated electron−hole pairs at the gap energy. These emit photons and return to the ground state.

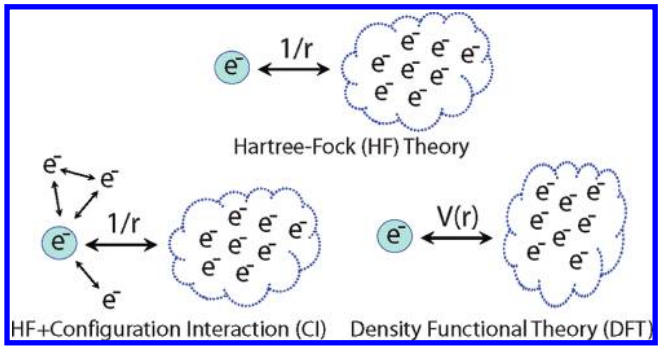

FIGURE 2. Illustration of single-particle HF theory and two alternative models for electron−hole correlations. In HF, every single electron interacts with the mean field created by the cloud of remaining electrons. CI adds correlation between electron pairs, triplets, etc. DFT builds an effective interaction potential that is different from $1/r$ and includes electron correlations within a modified single-particle description.

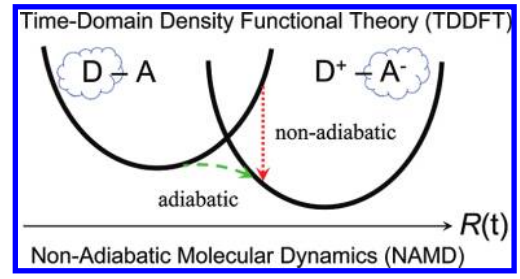

FIGURE 3. TDDFT combined with NAMD generates electron−phonon evolution. Electron density transfer between donor and acceptor is coupled to vibrational motion, $R(t)$. Transfer is adiabatic if the system remains in one electronic state. Nonadiabatic transfer occurs by hopping between states.

Electron−Electron Correlations Are Captured by Configuration Interaction. Electronic correlation is responsible for excitonic effects and can be very strong. It is added systematically to HF using configuration interaction (CI) and cluster expansions. The exact many-body wave function can be obtained, although at a very high computational expense. Configurations of two-body, three-body, etc. correlations, Figure 2, represent multiple excitons, whose properties are particularly important for QD photochemistry. CI evaluates electron correlations explicitly but can be applied only to small clusters.

Density Functional Theory Includes Electron Correlations within an Effective Single-Particle Model. DFT accounts for electron correlations indirectly. Justified by proof-of-principle showing that ground state properties can be obtained exactly from three-dimensional spatial density rather than multidimensional wave function, DFT replaces Coulomb interaction with a density functional, Figure 2. Kohn−Sham (KS) DFT ensures that density corresponds to a wave function. Excitonic electron−hole interactions are included in DFT implicitly through the functional. KS DFT is an effective single-particle theory. HF can be viewed as a special form of DFT that includes exact Pauli exchange and no electron correlation. As illustrated below, HF and DFT give different single-particle pictures. DFT is computationally inexpensive and works particularly well with extended systems that do not undergo complex chemical changes.

Time-Domain Density Functional Theory Evolves Electrons Driven by External Fields. TDDFT rigorously describes system's response to external perturbations, such as electro-magnetic fields and phonons, Figure 3. Linear response

TDDFT is frequently used to evaluate electronic excitation energies. Full TDDFT employed here propagates electron density explicitly in time. Taking full computational advantage of time-independent DFT, we use its solutions as a basis for our TDDFT calculations.[20]

Nonadiabatic Molecular Dynamics Evolves Atoms in Response to Changes in Electron Density. Classical-mechanical prescription for phonon dynamics in response to changes in electron density constitutes the quantum-backreaction problem,[21] and the combined electron−phonon evolution is called NAMD, Figure 3. Traditional MD is performed in a single, usually ground, electronic state. NAMD includes transitions between states. Most often, NAMD generates quantum-backreaction using surface hopping (SH), which stochastically correlates phonon dynamics with electronic states. Fewest switches SH (FSSH) minimizes hops and satisfies detailed balance between transitions up and down in energy, as required by thermodynamic equilibrium.[22] FSSH was implemented within TDDFT in ref 20.

Electronic Excitations in Semiconductor Quantum Dots

Photon absorption initiates complex electron−phonon dynamics in semiconductor QDs, Figure 1. One or several electrons can be promoted from valence band (VB) to conduction band (CB), depending on optical selection rules and electron−hole interaction strength.

Density Functional Theory Shows Broken Symmetries in Band Structure. Densities of states (DOS) for $Cd_{33}Se_{33}$, $Cd_{33}Se_{33}/Zn_{78}S_{78}$, and $Pb_{68}Se_{68}$ QDs obtained with DFT are shown in Figure 4. The first CB peak, as S-electron state in EMT, is clearly seen in both CdSe and PbSe QDs. The state is roughly spherically symmetric and is delocalized over the whole QD. Higher energy peaks can be attributed to P, D, etc. electronic levels, although state symmetries become harder to discern from state densities obtained by atomistic simulation.[16,23,24] The corresponding VB state structure is less pronounced, since the states are closer in energy. This agrees with EMT, which uses a higher effective mass for holes than electrons, particularly in CdSe.[11] Although DOS shows distinct peaks, they are separated only at low energies. Compared with EMT and tight-binding calculations that predict highly degenerate energy levels, *ab initio* results demonstrate that atomic structure, surface effects, core/shell coupling, thermal fluctuations, spin−orbit and Coulomb interactions break degeneracies and create complicated multilevel electronic structure. Atomistic pseudopotential calculations lead to similar conclusions.[17−19] Existence of multiple levels near band

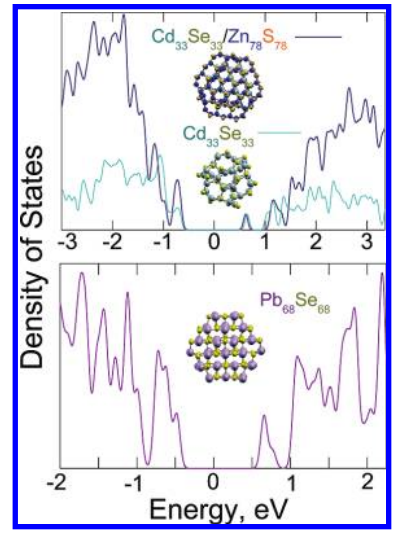

FIGURE 4. DOS of CdSe and PbSe QDs obtained by DFT. Top panel compares DOS of $Cd_{33}Se_{33}$ and core/shell $Cd_{33}Se_{33}/Zn_{78}S_{78}$. The lowest energy electron levels arise purely from the core, while bandgap hole levels contain shell contributions. PbSe DOS is more symmetric, bottom panel.

edge is supported by measurements with single PbS QDs, showing homogeneous broadening and complex structure of fluorescence spectra.[25] Photoluminescence blinking in single QDs may indicate that the photogenerated exciton is distributed over multiple on/off states. PbSe DOS is notably more symmetric than CdSe DOS. This is seen particularly well with peak heights. Zero-temperature energy gaps are underestimated relative to experiment, as typical with density-gradient functionals. The problem is attributed to incomplete elimination of self-interaction.[26] Nonlocal and NA corrections are routinely used to remedy the problem. For instance, hybrid functionals include portions of exact HF exchange. Bandgaps of core and core/shell CdSe QDs are similar, Figure 4, indicating that surface reconstruction is capable of saturating dangling bonds. ZnS has larger bandgap than CdSe. ZnS VB edge aligns with that of CdSe, while CB starts notable higher. Further discussion of shell, ligands, and other surface effects is given below.

Hartree−Fock Band Structure Provides a Reference Single-Particle Picture. HF DOS of CdSe and PbSe QDs[27] are shown in Figure 5. Since DFT accounts for electron correlations, while HF does not, one observes both close similarities and drastic differences between the HF and DFT data, compare Figures 4 and 5. Band structures of PbSe QDs are significantly more symmetric compared with CdSe in both cases. However, bandgaps predicted by HF are huge. Excitation energies computed by CI, Figure 6, are three times smaller than HF single-particle energy gaps, indicating the importance of electron−hole interactions. Small QDs provide good represen-

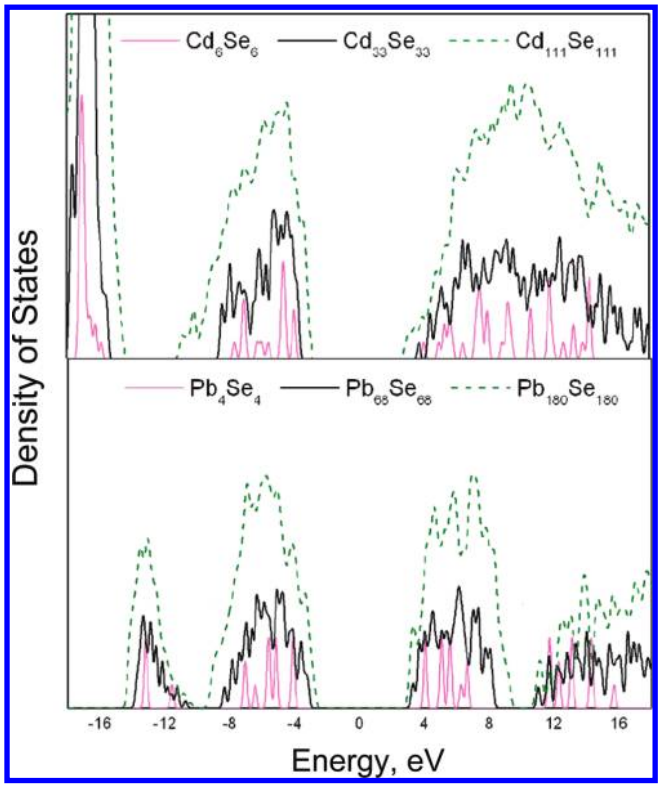

FIGURE 5. DOS of CdSe and PbSe QDs obtained by HF. Smaller QDs provide good approximations for larger QD DOS. Close similarities and dramatic differences between DOS of Figures 4 and 5 are discussed in the text.

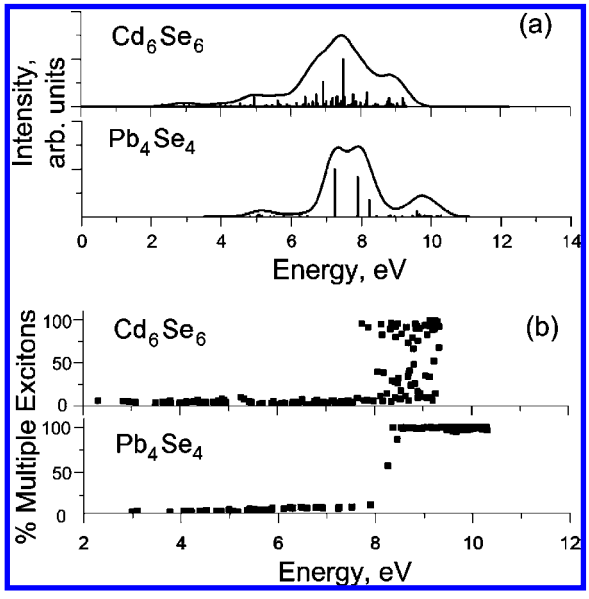

FIGURE 6. (a) Electronic absorption spectra and (b) electron/hole origin of photoexcited states of small CdSe and PbSe QDs, whose DOS are depicted in Figure 5. Very high-level *ab initio* CI calculations are used.

tation of large QD DOS, Figure 5. Hence, conclusions derived for the small dots using computationally demanding CI below should hold for larger dots, at least qualitatively. The electron and hole subbands in PbSe clusters have different atomic origins, independent of QD size. CdSe QD bands have mixed character, producing asymmetric band structure.

Excitonic Electron−Hole Interactions Are Strong in Small Clusters. Coulomb interaction between electrons and holes is very important in small QDs. It manifests itself very clearly in multiple exciton (ME) generation, which carries promise for photovoltaic applications.[11,13−16] If MEs can be created by absorption of a single high-energy photon, extra energy stored in the blue region of Sun's spectrum can be utilized to excite additional charge carriers rather than being lost to heat.[11] Figure 6 illustrates this effect. CI spectra for Cd_6Se_6 and Pb_4Se_4 are presented in Figure 6a. Because of lower symmetry, Cd_6Se_6 shows a complex spectrum with more allowed transitions.[27] Figure 6b shows ME contributions to excited states at different energies. Low-energy excitations are single excitons (SE). Minor ME contributions arise from electron correlation corrections to single-particle excited states. Sharp qualitative changes are seen at energies greater than twice the first excitation energy. Almost all highly excited states of PbSe become MEs. This direct mechanism of ME generation[27] explains how MEs can be obtained within picoseconds[14] and without electron−phonon relaxation bottleneck.[11,28,29] In contrast, CdSe exhibits mixtures of SEs, MEs, and superpositions thereof. SEs can generate MEs by impact ionization.[11,17,18] Superpositions can decay into MEs by phonon-induced dephasing.[14]

Direct photoexcitation of MEs is optically allowed due to electronic correlation. At single-particle level, only transitions involving one electron are possible. Mixing of SE and ME by electron−hole Coulomb interaction breaks selection rules forbidding ME transitions. As expected, SE transitions show significantly higher intensities than ME transitions, Figure 6a. The ME threshold in Pb_4Se_4 is at 2.8× the first excitation energy (E_{gap}). It is slightly higher in Cd_6Se_6. Threshold energies of $2.9E_{gap}$ and $2.5E_{gap}$ were observed in larger PbSe and CdSe QDs.[13] Experimental results,[14] along with theoretical estimates,[18] give the PbSe threshold energy at $2.1E_{gap}$. Theory[30] indicates that conclusions obtained for small QDs should remain valid with QDs up to 3 nm in diameter. In larger QDs, electronic correlation weakens due to increased electron−hole separation.

Phonon-Induced Dephasing of Electronic Excitations

Electron−phonon interactions give rise to two qualitatively different phenomena. Superpositions of electronic states dephase into uncorrelated states, conserving energy.[31] Energy is transferred to phonons during electron−phonon relaxation.[23,24]

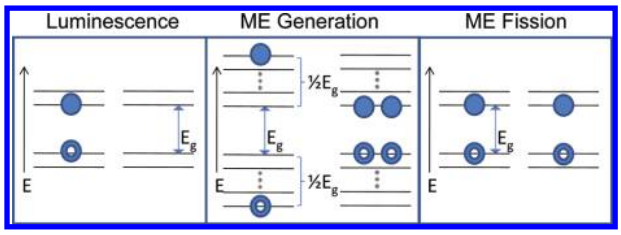

FIGURE 7. Diagram showing pairs of electronic states involved in light absorption/luminescence, ME generation, and ME fission. The state pairs form coherent superpositions that dephase by coupling to phonons. The dephasing times are given in Table 1.

This section focuses on dephasing that is responsible for optical linewidths, ME generation, and ME fission, see Figures 1 and 7. Pairs of states in Figure 7 form coherent superpositions that dephase by coupling to phonons. Table 1 presents dephasing times.

Optical Linewidths in Single Quantum Dots Are Determined by Electron−Phonon Interaction. Excluding inhomogeneous broadening associated with distributions of optically active species, intrinsic homogeneous linewidths, Γ, of optical transitions are inversely proportional to dephasing time, T_2. The latter includes excited-state lifetime, T_1, and pure-dephasing, T_2^*:

$$\Gamma = \frac{1}{T_2} = \frac{1}{2T_1} + \frac{1}{T_2^*} \quad (1)$$

Pure dephasing is associated with fluctuations of electronic levels due to coupling to phonons. For sufficiently long T_1, Γ is determined by T_2^*. In semiconductor QDs, first excited-state lifetimes are very long. Therefore, luminescence and lowest energy absorption linewidths are determined by pure-dephasing.

Dephasing between the ground and lowest energy excited states takes 10 fs, top row in Table 1. Lowering temperature from 300 to 100 K doubles the time. The corresponding linewidths, eq 1, are around 100 meV, in good agreement with experiment.[25] Debye-type relaxation attributed to reorientation of surface ligands may produce additional dephasing and increase optical linewidths.[32] Dephasing is faster in smaller QDs due to stronger electron−phonon coupling. Generally, coupling grows with decreasing system size. It is weak in bulk and strong in molecules and defects.[33]

TABLE 1. Times (fs) of Phonon-Induced Pure Dephasing between Pairs of Electronic States Involved in Light Absorption/Luminescence, ME Generation and ME Fission, Figure 7[a]

	$Si_{29}H_{24}$	$Cd_{33}Se_{33}$	$Pb_{68}Se_{68}$	$Pb_{16}Se_{16}$
luminescence	4/7	10/16	9/23	7/*b*
ME generation	4/7	5/9	5/11	4/*b*
ME fission	80/310	*b*	*b*	*b*

[a] Numbers before and after "/" correspond to temperatures of 300 and 100 K, respectively. [b] No available data.

Superpositions of Singly and Multiply Excited States Dephase Rapidly by Coupling to Phonons. Electron−hole interactions create superpositions of SEs and MEs, Figures 1 and 7. Such superpositions should decay primarily into MEs,[14] since exciting more electrons generates larger changes in QD electronic structure and stronger electron−phonon coupling. The lifetimes of SE/ME superpositions are given in the second row of Table 1. Since electronic origins of SEs and MEs differ significantly, the SE/ME dephasing times are ultrafast. Superpositions of SEs and MEs rapidly lose coherence, become uncorrelated, and evolve independently.[31,34]

Phonon-Induced Fission of Multiple Excitons Is Subpicosecond. With time, MEs break into incoherent combinations of SEs that can emit independently. Directly analogous singlet fission was observed in tetracene, anthracene, and other polyacene crystals.[35] Phonon-induced dephasing leading to ME fission in semiconductor QDs is much slower than dephasing responsible for optical linewidths and ME generation,[31] Table 1. The difference becomes more pronounced at lower temperatures. Linear response theory relates dephasing to phonon-induced fluctuations of the energy gap between the states. MEs and sums of SEs into which MEs break have similar energies and densities. Hence, gap fluctuations are small, and dephasing is slow. ME fission times are yet to be measured in semiconductor QDs. The calculated values agree with the singlet fission times observed in molecular systems.[35]

Electron−Phonon Relaxation

Quantization of electronic energy levels induced in QDs by spatial confinement can lead to mismatches between electronic gaps and phonon frequencies. Dramatic slowing of electron−phonon relaxation, known as phonon bottleneck,[11] can ensue. Large spacing between electronic levels is clearly seen in optical spectra.[25] Unexpectedly, relaxation times show a broad spread from 100 fs to 1 ns, depending on excitation.[36] Many time-resolved experiments show picosecond relaxation, similar to that observed in bulk.[28,29] Moreover, relaxation accelerates with decreasing QD size, even though electronic energy spacings increase. Recently, phonon bottleneck was observed under special conditions in carefully designed CdSe QDs.[12] By slowing electronic energy decay, phonon bottleneck can minimize losses during solar energy harvesting and allow generation of additional charge carriers.[11,13−15] Taking a step further beyond static EMT[11,14] and pseudopotential[17−19] calculations, time-domain theoret-

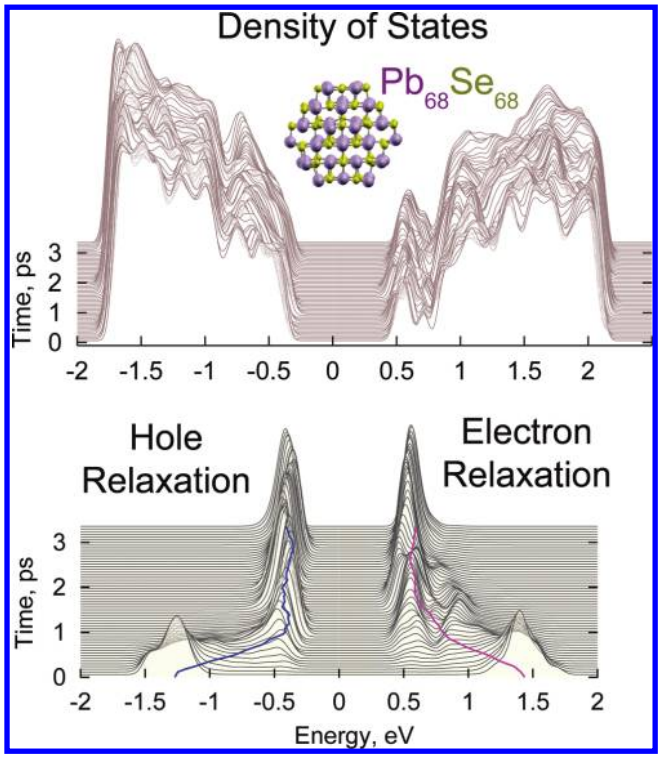

FIGURE 8. Evolution of DOS (top panel) and electron/hole energy relaxation (bottom panel) in $Pb_{68}Se_{68}$ at room temperature. The DOS fluctuates due to thermal atomic motions. Both electrons and holes relax within a picosecond. Holes decay faster than electrons due to higher DOS. The relaxation involves all states at energies in the range of the photoexcited and bandgap states.

ical studies[16,23,24] directly mimic time-resolved experiments and provide detailed atomistic description of the relaxation processes.

Relaxation at High Energies Is Ultrafast due to Large Electronic State Density. Phonon motions induce fluctuations in electronic DOS, as illustrated with $Pb_{68}Se_{68}$ in the top panel of Figure 8. The fluctuations are minor: CB and VB edges change by less than 0.1 eV and are significantly smoothed, Figures 4 and 8. Phonon motions mix states of different symmetries and reduce gaps between states. The bottom panel of Figure 8 presents NA dynamics of electron and hole relaxation mediated by coupling to phonons.[16,23,24] Charge carriers visit multiple states during relaxation, and no intermediate states play special roles. The population peaks created by photoexcitation spread to reappear near the bandgap. Relaxation is nearly complete within a picosecond, in agreement with experiment.[28,29] No phonon bottleneck is observed at high photoexcitation energies. Most likely transitions involve small amounts of energy that are close to phonon energies of 100−200 cm^{-1} (12−25 meV). This indicates that electronic energy gaps are small at high energies, explaining the absence of phonon bottleneck. Transitions involving larger amounts of energy and multiple phonon quanta do occur. Occasionally, up to 0.3−0.6 eV of electronic energy can be lost to phonons in single events.[16,23,24] Multiphonon relaxation proposed initially to rationalize ultrafast experimental data[28] is indeed seen in our simulation; however, faster resonant electron−phonon energy exchange is also efficient, particularly at higher energies.

Phonon Bottleneck Is Seen at Low Energies since Electronic States Are Widely Spaced. Our simulation[24] showed partial phonon bottleneck associated with final stages of electron relaxation in $Cd_{33}Se_{33}$. This result agrees with observed slowing of charge relaxation, as carriers approached band edge.[37] Recent experiments[12] detected nanosecond relaxation between P- and S-states of electrons injected into carefully designed multilayer CdSe QDs. The $Cd_{33}Se_{33}$ DOS in Figure 4 indicates that indeed only S-electron state is separated from the rest. Pure-dephasing time[34] between S- and P-states is shorter than transition time.[24] Therefore, TDDFT/NAMD applied to this transition must be augmented to include decoherence.[33] Analysis performed in ref 33 suggests that decoherence significantly decelerates relaxation. This expectation is closely related to quantum Zeno effect.[38] Relaxation involving dense state manifolds is not affected by coherence loss, because transitions occur faster than decoherence. Simulation of the final electronic transition in CdSe QDs is currently under way.

Relaxation Shows Temperature Dependence since It Is Promoted by Low-Frequency Phonons. Temperature dependence of carrier relaxation distinguishes phonon-induced processes from other channels, such as Auger scattering.[39] Experiments showed[28,40] that relaxation is much more temperature-dependent in PbSe than in CdSe QDs, where Auger processes are more effective. Temperature-activated relaxation was found in InAs/GaAs QDs.[41] Different temperature dependences suggest that phonons play important roles in most, but not all, QDs. Empirical pseudopotential calculations based on static lattice[19] indicate that PbSe relaxation accelerates with temperature in larger QDs and decelerates in smaller QDs. Time-domain approaches model carrier dynamics in semiconductor QDs directly.[16,23,24,42]

Figure 9a shows that phonon-induced relaxation of both electrons and holes in $Pb_{16}Se_{16}$ is temperature-dependent. More phonons are excited at higher temperatures, and carrier−phonon scattering is more frequent. NA electron−phonon coupling is proportional to phonon velocity and, hence, the square root of kinetic energy.[20,42] Since kinetic energy is proportional to temperature, one can expect that NA

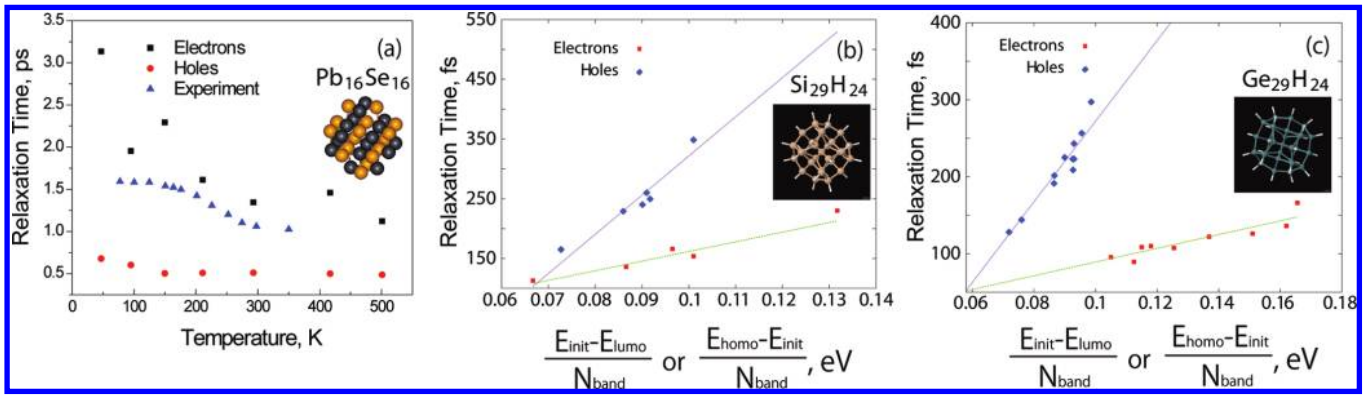

FIGURE 9. Electron and hole relaxation times in (a) $Pb_{16}Se_{16}$, (b) $Si_{29}H_{24}$, and (c) $Ge_{29}H_{24}$ QDs. Part a shows calculated and experimental relaxation times vs temperature. Parts b and c correlate calculated relaxation times with state energy spacing averaged over the relaxation energy range. Holes decay faster than electrons in PbSe due to their higher DOS, see Figures 4 and 8. Electrons decay faster than holes in the Si and Ge QDs due to higher DOS and involvement of surface modes, see Figure 10.

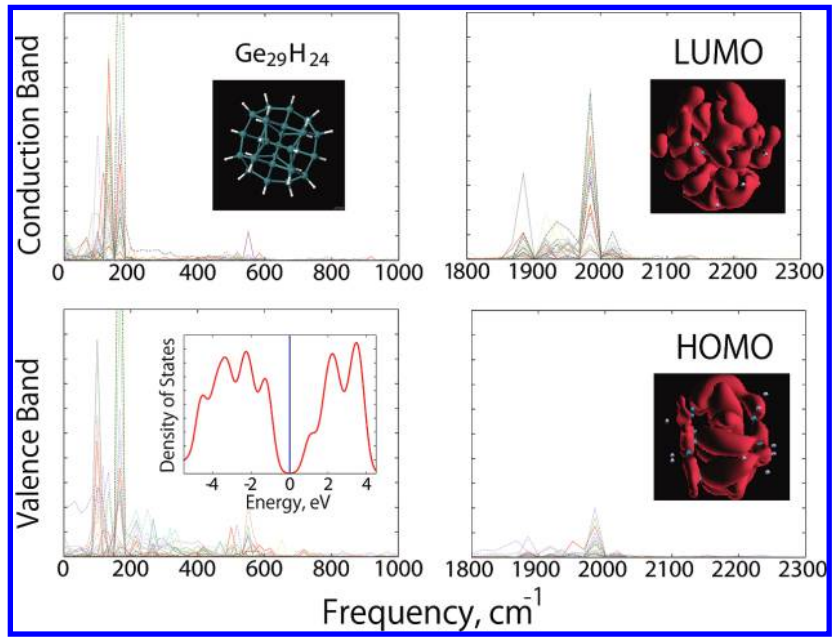

FIGURE 10. Frequencies of phonon modes that couple to CB and VB states in $Ge_{29}H_{24}$. The inserts show QD geometric structure, DOS, and HOMO/LUMO orbital densities. In Ge and Si QDs, electrons decay faster than holes, in contrast to PbSe and CdSe, see Figure 9, because electrons have higher DOS and couple more strongly to high-frequency surface modes. Coupling to surface modes is rationalized by larger surface delocalization of CB orbitals, for example, LUMO, than VB orbitals, for example, HOMO.

coupling varies as $T^{0.5}$. By Fermi's golden rule, relaxation rate is proportional to coupling squared,

$$k_F = \frac{2\pi}{\hbar}|V|^2\rho(E_{band}) \qquad (2)$$

Hence, relaxation rate and time should scale as T and T^{-1}, respectively. The results shown in Figure 9a deviate from this trend. Both electron and hole decay times are fitted to $T^{-0.4}$. The weaker dependence can be attributed to temperature variation of the electronic overlap contribution to NA coupling.[20] It decreases with temperature as $T^{-0.3}$ due to QD expansion. Although QD geometry is weakly temperature-dependent,[43] the coupling can strongly depend on expansion.[42]

The time-domain *ab initio* calculations show that primarily acoustic and to some extent optical phonons participate in the electron-phonon relaxation. More phonons are activated at higher temperature. Due to faster overall relaxation, temperature dependence is less evident with holes. Experimentally observed temperature variations[28,40,41] are explained by considering both phonon and Auger channels: at low temperatures, Auger relaxation dominates, while at higher temperatures, phonon relaxation becomes more efficient.

Higher Electronic State Density Facilitates Faster Relaxation. Electrons decay more slowly than holes in small PbSe QDs, Figure 9a. The difference is less pronounced in

larger QDs, Figure 8. In contrast, electrons decay more rapidly than holes in Si and Ge QDs, Figures 9b,c. These differences in relaxation rates can be rationalized by higher DOS of faster relaxing carriers, $\rho(E_{band})$, once again using Fermi's golden rule, eq 2. The linear correlations in Figures 9b,c follow eq 2, since the lifetime, *y*-axis, is inverse rate, and the average level spacing, *x*-axis, is inverse DOS. With average values of NA coupling, eq 2 fits the data up to a 1.5 prefactor.[44] The prefactor is rationalized by coupling fluctuations. It corrects for high transition probabilities at large coupling. The ratios of electron and hole relaxation rates in Figures 9b,c are described by Fermi's golden rule quantitatively with no adjustable parameters.

Auger Processes

Charge−phonon relaxation is closely tied with Auger scattering.[39] Coulomb interactions between electrons and holes confined within QDs induce charge-carrier relaxation and recombination. If electron and hole DOS are asymmetric, as with most QDs, Figures 4, 5, 8, and 10, rapid Auger energy exchange funnels excitation energy to faster relaxing carriers with higher DOS. For instance, holes are much denser than electrons in CdSe, top panels in Figures 4 and 5, and Auger processes are important.[29,39] Electrons relax faster than holes in Si and Ge QDs,[44] Figure 9. Hence, Auger processes should proceed in opposite directions in Si and Ge QDs compared with CdSe, PbSe, and GaAs QDs.[16,23,24] Electron and hole relaxations differ more in Ge than Si QDs.[44] Therefore, Auger relaxation should be more important in Ge QDs. Symmetric DOS renders the Auger channel inefficient, for instance, in PbSe, bottom panels of Figures 4 and 5. Both electrons and holes relax by direct coupling to phonons.[28,29]

Auger relaxation is efficient only when electrons and holes are coupled via Coulomb interaction. Time-resolved experiments in CdSe QDs show that intraband relaxation is fast even if holes are decoupled from electrons through either surface hole trapping or electron injection into neutral dots.[40] Decoupled carriers decay via phonons. Simultaneous relaxation by combination of electron−phonon and Auger pathways was addressed in ref 36. The importance of surface ligands and carrier separation was noted in ref 45. Only static atomistic calculations of Auger processes have been performed thus far.[17−19] Time-domain simulations are currently under way. They involve many states and are computationally demanding.

Surface Effects and Quantum Dot Charging

Surfaces create charge traps and provide high-frequency phonons associated with surface ligands.[45,46] "Magic" size clusters successfully self-heal.[16,23,24,27] However, traps associated with dangling chemical bonds, missing atoms, and other defects can be eliminated only by molecular ligands and core/shell designs.[12]

Core/Shell Designs Reduce Surface Defects. Surface passivation by inorganic shells or organic ligands may be expected to dramatically change QD DOS. To test this possibility, compare the DOS of $Cd_{33}Se_{33}$ and core/shell $Cd_{33}Se_{33}/Zn_{78}S_{78}$, top panel in Figure 4. If unpassivated QDs had preserved bulk structure, multiple unsaturated surface bonds would have introduced bandgap states. Surface reconstruction can eliminate gap states, particularly if surface atoms have no more than one dangling bond. Our calculations[16,23,24] show that surface reconstruction is maintained at finite temperatures. Reconstruction is subtle and preserves bulk topology. Remarkably, surface reconstruction is nearly equivalent to a shell layer, Figure 4. Because ZnS has a much larger bandgap than CdSe, band-edge states of the core/shell structure originate from the core. CdSe and CdSe/ZnS DOS differ significantly only at higher energies. Low-energy CB states are localized entirely on the core, while low-energy VB states have notable shell contributions. PbSe is much less susceptible to surface effects compared with CdSe. Surface reconstruction is less effective in eliminating gap states in small Si and Ge QDs,[44] which require hydrogen atoms or other ligands, Figures 9 and 10.

Ligands Saturate Dangling Bonds and Accelerate Electron−Phonon Relaxation. Ligand contribution to QD excitation dynamics is exemplified with Si and Ge QDs in Figures 9 and 10. *Ab initio* calculations showed[44] that quantum confinement makes electron and hole DOS more symmetric in Si and Ge QDs compared with bulk. Despite symmetric DOS, electrons decay faster than holes, Figure 9b,c. Asymmetric relaxation can be rationalized by stronger electron−phonon coupling in the CB, due to larger contributions of high-frequency phonons associated with Ge−H and Si−H surface bonds. Figure 10 shows spectral densities of phonon modes that couple to CB and VB states of $Ge_{29}H_{24}$. Low-frequency motions are Ge−Ge bond vibrations and show little difference between VB and CB, left panels. Asymmetry is clearly seen in high-frequency components that originate from Ge−H surface bonds, right panels in Figure 10. Even though low-frequency modes influence electronic energies more than high-frequency modes (compare amplitudes in left and right panels

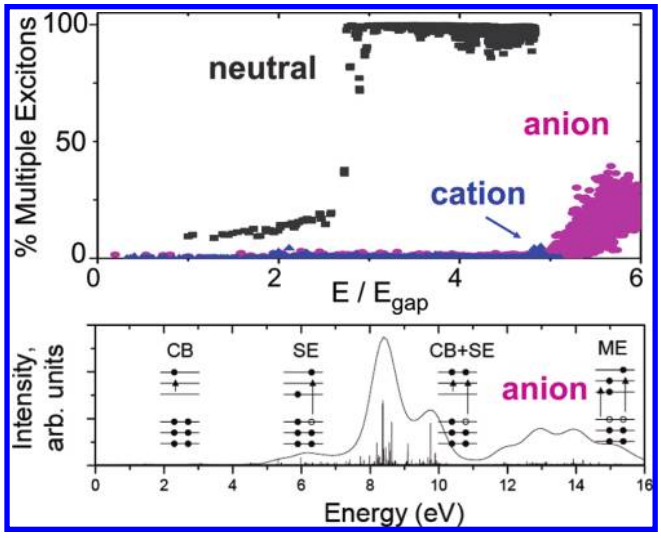

FIGURE 11. Contributions of MEs (top) to excited states of neutral, anionic, and cationic Pb_4Se_4 vs excitation energy relative to the lowest excitation, E_{gap}, of the neutral QDs. All excited states in neutral QDs become MEs at $2.5E_{gap}$. In contrast, small ME contributions appear in charged QDs at much higher energies. Electronic absorption spectrum (bottom) of anionic Pb_4Se_4. Inserts show electron−hole excitations that are responsible for different parts of the spectrum. Charging causes spectral blue-shift, compare with Figure 6a, and dramatically suppresses MEs due to appearance of new types of excitations involving the extra CB electron, see top panel.

of Figure 10), higher-frequency modes have faster velocities and accelerate charge relaxation through velocity dependence of NA coupling.[20] CB states of Ge are more delocalized onto the surface than VB states, see inserts in Figure 10. This is in contrast to CdSe, in which surface states contribute to VB and holes are easily trapped by ligands.[12,46]

Charges Dramatically Change Electronic Properties. Charging blue-shifts optical spectra, Figure 11, causing QD blinking.[47] Even though many low-energy excited states appear in charged QDs, these states are optically inactive. They accelerate nonradiative relaxation to the ground state. Electronic transitions inside VB and CB of charged QDs dominate low-energy excitations and push SEs and MEs to higher energies.[48] For instance, the first SE is at 2.9 eV in neutral Pb_4Se_4 and 4.2 eV in anion, compare Figures 6 and 11. Some ME character appears at 14 eV in anion,[48] while nearly 100% of MEs are seen at 8 eV in neutral Pb_4Se_4.[27] Anion excitations at 8 eV are mixtures of CB and SE transitions, rather than MEs. *Ab initio* atomistic calculations show that ME detection is much more difficult in charged QDs.[48]

Conclusions and Outlook

Ab initio modeling of excited-state dynamics in energy and time domains generates valuable insights into semiconductor QD properties. TDDFT combined with NAMD simulates complex evolutions of coupled electronic and vibrational degrees of freedom as it occurs in nature. Compared with EMT and tight-binding calculations that predict highly degenerate energy levels in QDs, *ab initio* calculations demonstrate that atomic structure, surface effects, core/shell interactions, thermal fluctuations, and Coulomb coupling break degeneracies and create complicated distributions of electronic levels. *Ab initio* descriptions directly illustrate nonideal processes and generate input for modifications and extensions of phenomenological models. They show that surface reconstruction significantly changes QD bandgaps. Ligand and shell layers saturate surface dangling bonds and alter high-energy regions of CB and VB, while ligand high-frequency modes create strong electron−phonon coupling. QD charging gives rise to intraband transitions that show little optical activity but dramatically modify the nature and energy of excited electronic states. Charging also blue-shifts absorption spectra and increases ME thresholds.

Electron−phonon interactions induce two distinct processes in QDs: dephasing and relaxation. Superpositions of electronic states, created by Coulomb interaction during photoexcitation and subsequent time evolution, dephase into incoherent mixtures of states. Dephasing is ultrafast if it involves electronic states with substantially different energies and spatial densities. Examples include superpositions of SEs and MEs and ground and excited states. ME fission into independent SEs occurs by dephasing that is much slower, since MEs are typically formed by SEs that are close in energy. Time-domain modeling of electron−phonon relaxation unified two seemingly contradicting experimental observations: despite large spacings between optical lines, phonon bottleneck to electron−phonon relaxation exists only under very special conditions. Except for lowest excitation energies, electronic energy spacing matches phonon frequencies. QD spectra are composed of multiple individual excitations that combine into distinct bands according to optical selection rules. Selection rules are much less stringent for electron−phonon transitions. Even though relatively few excitations are strongly optically active, most excited electronic states participate in phonon relaxation.

Rapid development of *ab initio* approaches forms a solid foundation for further simulation advances in the near future. Auger processes are particularly important in nanoscale materials. At this point, they have been modeled only by time-independent phenomenological and pseudopotential methods. Time-domain simulations of Auger processes involve many electronic states. This computational challenge is currently

being overcome using sparse matrix techniques. The results reviewed above are limited to small QDs and a few systems. With increased computational power, the current methods will be applied to larger QDs and more diverse materials involving realistic ligands, surface defects, and variable core/shell compositions.[49] Longer-scale simulations of luminescence quenching and phonon bottleneck will become possible. Photovoltaic assemblies of QDs with other materials, such as molecular chromophores, polymers, and inorganic semiconductors present new theoretical questions. The issues raised here with electronic states in semiconductor QDs find close similarities with spin states and metallic QDs. *Ab initio* approaches in time and energy domains will greatly advance our understanding of the QD properties that govern solar energy harvesting and many other applications.

The author is indebted to his colleagues and collaborators. Particular gratitude is expressed to Dr. Svetlana Kilina for electron−phonon relaxation work, Dr. Hideyuki Kamisaka and Angeline Madrid for dephasing studies, Dr. Christine Isborn for excited state investigations, Dr. Kim Hyeon-Deuk for Auger developments, and Sean Fischer for comments on the manuscript. The research was supported by grants from NSF (Grant CHE-0701517), DOE (Grant DE-FG02-05ER15755), and ACS PRF (Grant 41436-AC6).

BIOGRAPHICAL INFORMATION

Oleg Prezhdo obtained Diploma in Theoretical Chemistry in 1991 from Kharkov National University, Ukraine, working on many-body electronic structure theory and electron-vibrational dynamics under Anatoly Luzanov. From 1991 to 1993, he developed a continuum model of molecular solvation with Stanislav Tyurin in Kharkov Polytechnic University. Having moved to the U.S.A. in the fall of 1993, he completed his Ph.D. on "Quantum-classical approaches for simulation of nonadiabatic chemical dynamics in solution" under Peter Rossky at UT-Austin in 1997. After a brief postdoctoral fellowship with John Tully at Yale, where he worked on constrained density-functional theory for electron transfer, he moved to University of Washington in Seattle in 1998. In 2002, he was promoted to Associate Professor and in 2005 to Full Professor. In 2008, he became a Senior Editor of the *Journal of Physical Chemistry*. His current research interests range from the fundamental aspects of semiclassical and nonadiabatic dynamics to time-domain density functional theory to photoexcitations in quantum dots, carbon nanotubes, and molecule−bulk interfaces to order−disorder transitions in electro-optic polymers and to the biological catch-bond.

FOOTNOTES

*E-mail: prezhdo@u.washington.edu.

REFERENCES

1 Milliron, D. J.; Hughes, S. M.; Cui, Y.; Manna, L.; Li, J. B.; Wang, L. W.; Alivisatos, A. P. Colloidal nanocrystal heterostructures with linear and branched topology. *Nature* **2004**, *430* (6996), 190–195.

2 Kilin, D. S.; Prezhdo, O. V.; Xia, Y. Shape-controlled synthesis of silver nanoparticles: Ab initio study of preferential surface coordination with citric acid. *Chem. Phys. Lett.* **2008**, *458* (1−3), 113–116.

3 Coe, S.; Woo, W. K.; Bawendi, M.; Bulovic, V. Electroluminescence from single monolayers of nanocrystals in molecular organic devices. *Nature* **2002**, *420*, 800–803.

4 Talapin, D. V.; Murray, C. B. PbSe nanocrystal solids for n- and p-channel thin film field-effect transistors. *Science* **2005**, *310*, 86–89.

5 Klimov, V. I.; Mikhailovsky, A. A.; Xu, S.; Malko, A.; Hollingsworth, J. A.; Leatherdale, C. A.; Eisler, H. J.; Bawendi, M. G. Optical gain and stimulated emission in nanocrystal quantum dots. *Science* **2000**, *290*, 314–317.

6 Farahani, J. N.; Pohl, D. W.; Eisler, H. J.; Hecht, B. Single quantum dot coupled to a scanning optical antenna: A tunable superemitter. *Phys. Rev. Lett.* **2005**, *95*, 017402.

7 Dahan, M.; Levi, S.; Luccardini, C.; Rostaing, P.; Riveau, B.; Triller, A. Diffusion dynamics of glycine receptors revealed by single-quantum dot tracking. *Science* **2003**, *302*, 442–445.

8 Kilin, D. S.; Tsemekhman, K. L.; Kilina, S. V.; Prezhdo, O. V. Photoinduced conductivity of a porphyrin-gold composite nanowire. *J. Phys. Chem. A* **2009**, *113*, 4549–4556.

9 Berezovsky, J.; Mikkelsen, M. H.; Stoltz, N. G.; Coldren, L. A.; Awschalom, D. D. Picosecond coherent optical manipulation of a single electron spin in a quantum dot. *Science* **2008**, *320*, 349–352.

10 Scheibner, R.; Buhmann, H.; Reuter, D.; Kiselev, M. N.; Molenkamp, L. W. Thermopower of a Kondo spin-correlated quantum dot. *Phys. Rev. Lett.* **2005**, *95*, 176602.

11 Nozik, A. J. Spectroscopy and hot electron relaxation dynamics in semiconductor quantum wells and quantum dots. *Annu. Rev. Phys. Chem.* **2001**, *52*, 193–231.

12 Pandey, A.; Guyot-Sionnest, P. Slow electron cooling in colloidal quantum dots. *Science* **2008**, *322*, 929–932.

13 Schaller, R. D.; Klimov, V. I. High efficiency carrier multiplication in PbSe nanocrystals: Implications for solar energy conversion. *Phys. Rev. Lett.* **2004**, *92*, 186601.

14 Ellingson, R. J.; Beard, M. C.; Johnson, J. C.; Yu, P. R.; Micic, O. I.; Nozik, A. J.; Shabaev, A.; Efros, A. L. Highly efficient multiple exciton generation in colloidal PbSe and PbS quantum dots. *Nano Lett.* **2005**, *5*, 865–871.

15 McGuire, J. A.; Joo, J.; Pietryga, J. M.; Schaller, R. D.; Klimov, V. I. New aspects of carrier multiplication in semiconductor nanocrystals. *Acc. Chem. Res.* **2008**, *41*, 1810–1819.

16 Prezhdo, O. V. Multiple excitons and the electron-phonon bottleneck in semiconductor quantum dots: An ab initio perspective. *Chem. Phys. Lett.* **2008**, *460* (1−3), 1–9.

17 Wang, L. W.; Califano, M.; Zunger, A.; Franceschetti, A. Pseudopotential theory of Auger processes in CdSe quantum dots. *Phys. Rev. Lett.* **2003**, *91*, 056404.

18 Franceschetti, A.; An, J. M.; Zunger, A. Impact ionization can explain carrier multiplication in PbSe quantum dots. *Nano Lett.* **2006**, *6*, 2191–2195.

19 An, J. M.; Califano, M.; Franceschetti, A.; Zunger, A. Excited-state relaxation in PbSe quantum dots. *J. Chem. Phys.* **2008**, *128*, 164720.

20 Craig, C. F.; Duncan, W. R.; Prezhdo, O. V. Trajectory surface hopping in the time-dependent Kohn-Sham approach for electron-nuclear dynamics. *Phys. Rev. Lett.* **2005**, *95*, 163001.

21 Prezhdo, O. V.; Kisil, V. V. Mixing quantum and classical mechanics. *Phys. Rev. A* **1997**, *56*, 162–175.

22 Parahdekar, P. V.; Tully, J. C. Mixed quantum-classical equilibrium. *J. Chem. Phys.* **2005**, *122*, 094102.

23 Kilina, S. V.; Kilin, D. S.; Craig, C. F.; Prezhdo, O. V. Ab initio time-domain study of phonon-assisted relaxation of charge carriers in a PbSe quantum dot. *J. Phys. Chem. C* **2007**, *111*, 4871–4878.

24 Kilina, S. V.; Kilin, D. S.; Prezhdo, O. V. Breaking the phonon bottleneck in PbSe and CdSe quantum dots: Time-domain density functional theory of charge carrier relaxation. *ACS Nano* **2009**, *3*, 93–99.

25 Peterson, J. J.; Krauss, T. D. Fluorescence spectroscopy of single lead sulfide quantum dots. *Nano Lett.* **2006**, *6*, 510–514.

26 Prezhdo, O. V. Assessment of theoretical approaches to the evaluation of dipole moments of chromophores for nonlinear optics. *Adv. Mater.* **2002**, *14*, 592–600.

27 Isborn, C. M.; Kilina, S. V.; Li, X.; Prezhdo, O. V. Generation of multiple rxcitons in PbSe and CdSe quantum dots by direct photoexcitation: first-principles calculations. *J. Phys. Chem. C* **2008**, *112*, 18291–18294.

28 Schaller, R. D.; Pietryga, J. M.; Goupalov, S. V.; Petruska, M. A.; Ivanov, S. A.; Klimov, V. I. Breaking the phonon bottleneck in semiconductor nanocrystals via

multiphonon emission induced by intrinsic nonadiabatic interactions. *Phys. Rev. Lett.* **2005**, *95*, 196401.

29 Cooney, R. R.; Sewall, S. L.; Anderson, K. E. H.; Dias, E. A.; Kambhampati, P. Breaking the phonon bottleneck for holes in semiconductor quantum dots. *Phys. Rev. Lett.* **2007**, *98*, 177403.

30 Rabani, E.; Baer, R. Distribution of multiexciton generation rates in CdSe and InAs nanocrystals. *Nano Lett.* **2008**, *8*, 4488–4492.

31 Madrid, A. B.; Kim, H.-D.; Prezhdo, O. V. Phonon-induced dephasing of excitons in semiconductor quantum dots: Multiple exciton generation, fission, and luminescence. *ACS Nano* **2009**, *3*, 2487–2494.

32 Salvador, M. R.; Hines, M. A.; Scholes, G. D. Exciton-bath coupling and inhomogeneous broadening in the optical spectroscopy of semiconductor quantum dots. *J. Chem. Phys.* **2003**, *118*, 9380–9388.

33 Habenicht, B. F.; Prezhdo, O. V. Nonradiative quenching of fluorescence in a semiconducting carbon nanotube: A time-domain ab initio study. *Phys. Rev. Lett.* **2008**, *100*, 197402.

34 Kamisaka, H.; Kilina, S. V.; Yamashita, K.; Prezhdo, O. V. Ultrafast vibrationally-induced dephasing of electronic excitations in PbSe quantum dots. *Nano Lett.* **2006**, *6*, 2295–2300.

35 Lanzani, G.; Cerullo, G.; Zavelani-Rossi, M.; De Silvestri, S.; Comoretto, D.; Musso, G.; Dellepiane, G. Triplet-exciton generation mechanism in a new soluble (red-phase) polydiacetylene. *Phys. Rev. Lett.* **2001**, *87*, 187402.

36 Cooney, R. R.; Sewall, S. L.; Dias, E. A.; Sagar, D. M.; Anderson, K. E. H.; Kambhampati, P. Unified picture of electron and hole relaxation pathways in semiconductor quantum dots. *Phys. Rev. B* **2007**, *75*, 245311.

37 Xu, S.; Mikhailovsky, A. A.; Hollingsworth, J. A.; Klimov, V. I. Hole intraband relaxation in strongly confined quantum dots: Revisiting the "phonon bottleneck" problem. *Phys. Rev. B* **2002**, *65*, 045319.

38 Prezhdo, O. V.; Rossky, P. J. Quantum decoherence and short time solvent response. *Phys. Rev. Lett.* **1998**, *81*, 5294–5297.

39 Efros, A. L.; Kharchenko, V. A.; Rosen, M. Breaking the phonon bottleneck in nanometer quantum dots - role of Auger-like processes. *Solid State Commun.* **1995**, *93*, 281–284.

40 Guyot-Sionnest, P.; Wehrenberg, B. L.; Yu, D. Intraband relaxation in CdSe nanocrystals and the strong influence of the surface ligands. *J. Chem. Phys.* **2005**, *123*, 074709.

41 Menzel, S.; Zibik, E. A.; Aivaliotis, P.; Cockburn, J. W.; Wilson, L. R.; Steer, M. J. Evidence for nonadiabatic electron-phonon intraband scattering in self-assembled quantum dots. *Phys. Rev. B* **2008**, *77*, 153302.

42 Bao, H.; Habenicht, B. F.; Prezhdo, O. V.; Ruan, X. Temperature dependence of hot-carrier relaxation in PbSe nanocrystals: An ab initio study. *Phys. Rev. B* **2009**, *79*, 235306.

43 Kamisaka, H.; Kilina, S. V.; Yamashita, K.; Prezhdo, O. V. Ab initio study of temperature and pressure dependence of energy and phonon-induced dephasing of electronic excitations in CdSe and PbSe quantum dots. *J. Phys. Chem. C* **2008**, *112*, 7800–7808.

44 Kim, H.-D. Madrid, A. B. Prezhdo, O. V. Symmetric band structures and asymmetric ultrafast electron and hole relaxations in silicon and germanium quantum dots: Time-domain ab initio simulation, *Dalton Trans.* **2009**, available online, DOI: 10.1039/b909267f.

45 Guyot-Sionnest, P.; Wehrenberg, B.; Yu, D. Intraband relaxation in CdSe nanocrystals and the strong influence of the surface ligands. *J. Chem. Phys.* **2005**, *123*, 074709.

46 Kilina, S.; Ivanov, S.; Tretiak, S. Effect of surface ligands on optical and electronic spectra of semiconductor nanoclusters. *J. Am. Chem. Soc.* **2009**, *131*, 7717–7726.

47 Nirmal, M.; Dabbousi, B. O.; Bawendi, M. G.; Macklin, J. J.; Trautman, J. K.; Harris, T. D.; Brus, L. E. Fluorescence intermittency in single cadmium selenide nanocrystals. *Nature* **1996**, *383*, 802–804.

48 Isborn, C. M.; Prezhdo, O. V. Charging quenches multiple exciton generation in semiconductor nanocrystals: First-principles calculations on small PbSe clusters. *J. Phys. Chem. C* **2009**, *113*, 12617–12621.

49 Wang, X.; Ren, X.; Kahen, K.; Hahn, M. A.; Rajeswaran, M.; Maccagnano-Zacher, S.; Silcox, J.; Cragg, G. E.; Efros, A. L.; Krauss, T. D. Non-blinking semiconductor nanocrystals. *Nature* **2009**, *459*, 686–689.